Chemical Science

EDGE ARTICLE

View Article Online
View Journal | View Issue

Cite this: *Chem. Sci.*, 2019, **10**, 773

All publication charges for this article have been paid for by the Royal Society of Chemistry

Received 27th August 2018
Accepted 21st October 2018

DOI: 10.1039/c8sc03821j

rsc.li/chemical-science

Hexakis(2,3,6-tri-*O*-methyl)-α-cyclodextrin–I_5^- complex in aqueous I^-/I_3^- thermocells and enhancement in the Seebeck coefficient†

Yimin Liang,[a] Teppei Yamada, *[ab] Hongyao Zhou[a] and Nobuo Kimizuka [ab]

A large Seebeck coefficient (S_e) of 1.9 mV K^{-1} was recorded for the I^-/I_3^- thermocell by utilizing the host-guest complexation of hexakis(2,3,6-tri-*O*-methyl)-α-cyclodextrin (Me_{18}-α-CD) with the oxidized iodide species. The thermocell measurement and UV-vis spectroscopy unveiled the formation of an Me_{18}-α-CD–pentaiodide (I_5^-) complex, which is in remarkable contrast to the triiodide complex α-CD–I_3^- previously reported. Although the precipitation of the α-CD–I_3^- complex in the presence of an electrolyte such as potassium chloride is a problem in thermocells, this issue was solved by using Me_{18}-α-CD as a host compound. The absence of precipitation in the Me_{18}-α-CD and I^-/I_3^- system containing potassium chloride not only improved the S_e of the I^-/I_3^- thermocell, but also significantly enhanced the temporal stability of its power output. This is the first observation that I_5^- species is formed in aqueous solution in a thermocell. Furthermore, the solution equilibrium of the redox couples was controlled by tuning the chemical structure of the host compounds. Thus, the integration of host-guest chemistry with redox couples extends the application of thermocells.

Introduction

Thermo-electric conversion based on the Seebeck effect has attracted much interest due to its potential to retrieve waste heat and convert it to electricity, which provides a promising way to reduce the consumption of fossil fuel. Accordingly, semiconductor-based devices have been utilized as the main thermo-electric materials for many years. However, their small S_e limits their development.[1–5] Thermocells, often referred to as thermo-electrochemical cells or thermo-galvanic cells, offer an alternative approach for the design of thermo-electric devices, which have attracted increasing attention due to their relatively high S_e and low cost.[6–8]

Thermocells are composed of a redox pair that is dissolved into the electrolyte. As reviewed by Quikenden, Pringle *et al.*, various strategies have been devoted to improving the performance of thermocells, and their S_e reached up to 1.4 mV K^{-1} using Pt electrodes and an aqueous solution of $[Fe(CN)_6]^{3-/4-}$.[9–11] Recently, carbon nanotubes were utilized as electrodes and the conversion efficiency of the thermocell was enhanced to 3.95% relative to the Carnot cycle.[12–14] Ionic liquid-based thermocells have also been extensively studied, which exhibited a high S_e of 2.2 mV K^{-1} in a wide temperature range.[15–17] However, strategies to improve the figure-of-merit value is still required for the practical usage of thermocells.

We recently reported the concept of a supramolecular thermocell, which was demonstrated by introducing α-cyclodextrin (α-CD, Fig. S1a†) as a molecular host to the I^-/I_3^- thermocell. α-CD selectively captured the hydrophobic I_3^- anion, which led to a significant enhancement of S_e from 0.8 to 1.4 mV K^{-1}.[18] The addition of KCl as the supporting electrolyte resulted in the precipitation of the α-CD–I_3^- complex in the lower-temperature cells, which further increased the S_e value to *ca.* 2 mV K^{-1}. Polymers such as starch and poly(vinylpyrrolidone) also served as host matrices, which resulted in an increase in S_e to 1.5 and 1.2 mV K^{-1}, respectively.[19] This host–guest approach is applicable to various types of redox species and its effect is independent of the type of electrode. This was useful in improving the S_e value in thermocells, and the highest S_e of *ca.* 2 mV K^{-1} was achieved for the precipitation–dissolution equilibrium system of α-CD–I_3^- in aqueous KCl.

Although the addition of KCl was desirable to increase the conductivity of the electrochemical thermocell, the precipitation observed for the α-CD–I_3^- system decreased the diffusion ratio of the redox species and also impaired the durability of the thermocell. Thus, to solve this issue, it is essential to develop host molecules that show enhanced stability with the inclusion complex in aqueous electrolyte. Herein, we report the use of hexakis(2,3,6-tri-*O*-methyl)-α-cyclodextrin (Me_{18}-α-CD, Fig. S1c†) as a suitable host molecule for I^-/I_3^- thermocells. The aqueous

[a]*Division of Chemistry and Biochemistry, Graduate School of Engineering, Kyushu University, Motooka 744, Nishi-ku, Fukuoka 819-0395, Japan. E-mail: teppei343@gmail.com*

[b]*Center for Molecular Systems, Kyushu University, Motooka 744, Nishi-ku, Fukuoka 819-0395, Japan*

† Electronic supplementary information (ESI) available. See DOI: 10.1039/c8sc03821j

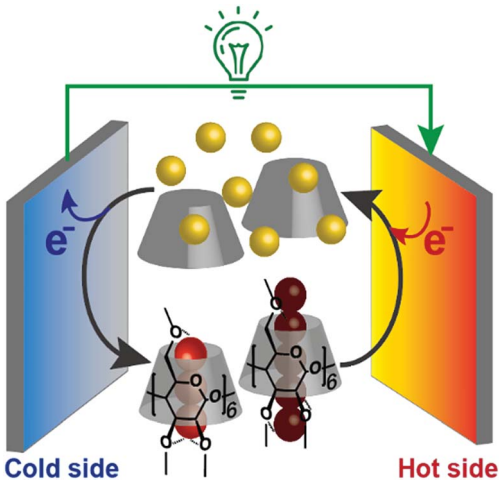

Fig. 1 Schematic of a supramolecular thermocell composed of I^- (yellow balls), I_3^- (trio of red balls), I_5^- (five connected dark red balls) and Me_{18}-α-CD (gray cone-shaped cylinder).

solution of Me_{18}-α-CD and iodide showed high stability and no precipitation was observed even in the presence of supporting electrolyte. The S_e of the thermocell reached 1.92 mV K^{-1}, which is the highest value reported to date for homogeneous I^-/I_3^- thermocells.

In addition, we found that this system showed an unusual off-stoichiometric interaction between Me_{18}-α-CD and I_3^-, and the formation of Me_{18}-α-CD–pentaiodide (I_5^-) complex was demonstrated for the first time. It should be noted that the formation of I_5^- species in aqueous solution has never been confirmed, and its presence has been only reported for solid crystals.[20–23] This result shows the design of proper host molecules leads to superior thermoelectric conversion (Fig. 1).

Results and discussion

Thermocell measurement

To investigate the effect of host–guest interaction, I^-/I_3^- thermocells were prepared using various concentrations of Me_{18}-α-CD. The concentration of the redox couple was kept same as that in the previous study ([KI] = 10 mM and $[I_3^-]$ = 2.5 mM).[18] In contrast to the previous α-CD–I^-/I_3^- system, the present Me_{18}-α-CD did not cause precipitation, even in the presence of KCl. The detail of the experimental procedure is described in the SI. The open circuit voltage (V_{oc}) of the cell between the hot and cold electrodes corresponds to the generating voltage of the cell. The temperature dependence of V_{oc} at varied concentrations of hosts is shown in Fig. 2a. The V_{oc} values were proportional to the temperature difference (ΔT), where the slope of the line corresponds to the Seebeck coefficient. That is, a high S_e value indicates a large voltage with the same temperature difference. In Fig. 2b, the obtained S_e was plotted as a function of the Me_{18}-α-CD and α-CD concentration. The data for the α-CD–I^-/I_3^- system was also shown for comparison. The S_e value obtained without hosts was 0.84 mV K^{-1}, which confirms the reproducibility of the previous study (0.86 mV K^{-1}).[18] In the case

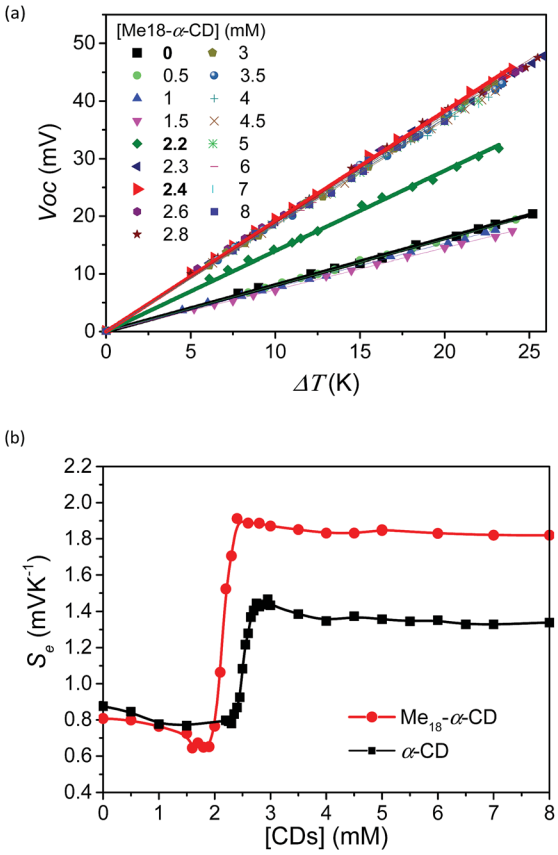

Fig. 2 (a) Plots of V_{oc} and ΔT with various Me_{18}-α-CD concentrations. $[KI]_0$ = 12.5 mM and $[I_2]_0$ = 2.5 mM. (b) Seebeck coefficient estimated from the slope of (a) with various concentrations of Me_{18}-α-CD (red circles) and α-CD (black squares) in the thermocells. The margin of error for each point was less than 0.02 mV K^{-1}.

of the Me_{18}-α-CD–I^-/I_3^- system, its S_e value was almost constant below the Me_{18}-α-CD concentration of 1.5 mM, while a drastic increase was observed above the concentration of 2.0 mM. The high S_e value was maintained above the concentration of *ca.* 2.4 mM. The maximum S_e of 1.92 mV K^{-1} was observed at the concentration of 2.2 mM, which is 1.08 mV K^{-1} higher than that without host molecules. This value is also *ca.* 0.5 mV K^{-1} higher than that obtained from the pristine α-CD–I^-/I_3^- cell system in the absence of KCl and is the highest value observed for homogeneous I^-/I_3^- thermocells. Although we reported a slightly higher S_e value of 1.97 mV K^{-1} for inhomogeneous precipitate–dissolution equilibrium mixtures caused by the addition of KCl to the α-CD–I^-/I_3^- thermocell, the presence of these precipitates significantly decreased its durability.[18]

An inflection point was observed for the curve at [Me_{18}-α-CD] = *ca.* 2.1 mM, which is well below that observed for α-CD (*ca.* 2.5 mM). In the case of α-CD, it stoichiometrically captures I_3^-, thus the concentration of the inflection point was almost the same as the initial concentration of I_3^-. The observed shift in the inflection point for Me_{18}-α-CD reflects the formation of complexes with different stoichiometries. As discussed below, the observed shift is derived from the complexation of Me_{18}-α-CD with I_5^- species.

Isothermal titration calorimetry

The stoichiometry of Me_{18}-α-CD and the polyiodide anion was investigated by isothermal titration calorimetry (ITC) (Fig. 3a). In the case of pristine α-CD, the inflection point of the ITC curve for α-CD with I_3^- was observed at *ca.* 1 : 1, which reflects the 1 : 1 complexation between I_3^- and α-CD.[18,24–26] In contrast, the inflection point of the ITC curve for Me_{18}-α-CD with I_3^- was *ca.* 1.2 : 1 at 10 °C, which further shifted to 1.3 : 1 with an increase in temperature. This result shows that the interaction of two I_3^- molecules with one Me_{18}-α-CD is involved. The most probable reaction is the encapsulation of the I_5^- ion according to the eqn (1) and (2). The formation of I_5^- ions in aqueous Me_{18}-α-CD is supported by the UV-Vis and Raman spectral measurements described later.

$$Me_{18}\text{-α-CD} + I_3^- \rightleftharpoons Me_{18}\text{-α-CD–}I_3^- \quad (1)$$

$$Me_{18}\text{-α-CD–}I_3^- + I_3^- \rightleftharpoons Me_{18}\text{-α-CD–}I_5^- + I^- \quad (2)$$

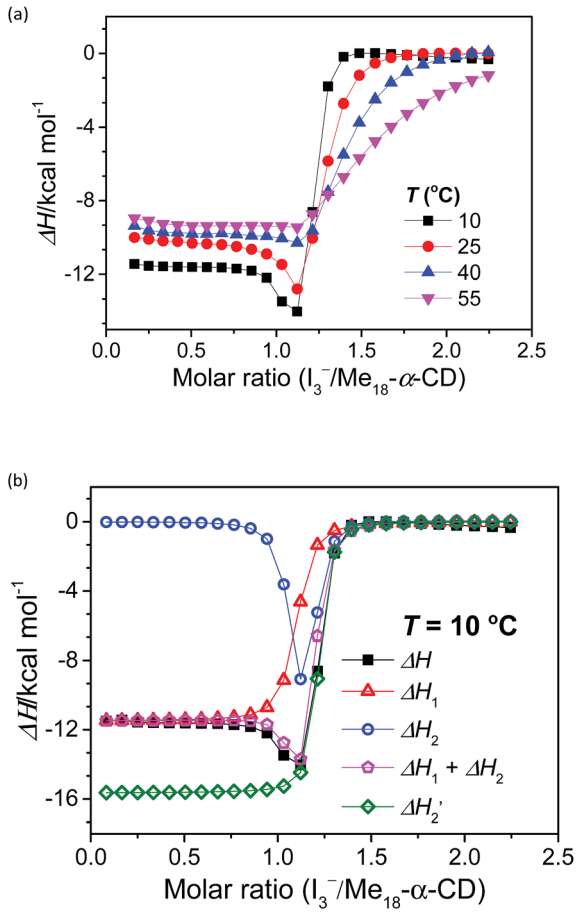

Fig. 3 (a) ITC curves of the aqueous solutions of I_3^- to Me_{18}-α-CD at various temperatures. (b) Optimum fitting ΔH_1 (red triangles), ΔH_2 (blue circles), sum of ΔH_1 and ΔH_2 (pink pentagons) and experimental result (black squares) of I_3^-/Me_{18}-α-CD titration at 10 °C. $\Delta H_2'$ (green diamonds) is a hypothetical ITC curve for the second binding stage generated by the SSIS model with the absence of the initial binding stage. The enthalpy change in the figures is normalized.

Since eqn (2) is an equilibrium reaction, the encapsulation reaction occurs at a high concentration of I_3^-. The ITC curves in Fig. 3a exhibit a hump of ΔH at the molar ratio between 0.8 to 1.1 eq., which can be attributed to the encapsulation of I_5^-.

To gain insight into the unique ITC data, curve fitting was executed. In the case of pristine α-CD, the ITC curve could be fitted with a simple 1 : 1 binding model between the host and I_3^- (a simple set of identical sites, SSIS), as reported previously.[18,24–26] In contrast, the SSIS model did not fit the ITC curve obtained for the Me_{18}-α-CD–I^-/I_3^- system (Fig. 3a). The fitting was not satisfactory even by applying the TSIS (two sets of independent sites) model, in which two types of sites bind independently to the guest molecules. These observations indicate that the second binding reaction in eqn (2) occurs cooperatively with the complexation between I_3^- and Me_{18}-α-CD (eqn (1)). We therefore fitted the ITC curve to the model reported by Kataoka *et al.*, which is a modified model based on the SSIS.[27] In this model, the concentration of the substance in the second reaction is generated by the initial reaction, and the experimental curve in Fig. 3a was fitted by the simultaneous control of these two interactions. The details of the fitting are revealed in the ESI.† As shown in Fig. 3b, the experimental ITC curve was successively fitted by the sum of ΔH_1 and ΔH_2 derived from the enthalpy changes according to eqn (1) and (2), respectively. The thermodynamic parameters are shown in Table S3.† The ITC curve of the initial binding stage, *i.e.*, I_3^- into Me_{18}-α-CD is presented in the red triangles in Fig. 3b. The shift in the stoichiometry from 1 : 1 to *ca.* 1.2 : 1 for the initial bonding stage should be attributed to the contribution of the second binding stage, which consumed a fraction of added I_3^-.

The complexation enthalpy between Me_{18}-α-CD and I_3^- at various temperatures was extracted in Fig. 4a. The binding constants (K) of Me_{18}-α-CD and I_3^- were estimated by these fittings and plotted in Fig. 4b. The K of pristine α-CD was also plotted in the figure, which is *ca.* 25 times larger at 10 °C than that observed at 55 °C, as reported previously.[18] On the other hand, Me_{18}-α-CD showed remarkable temperature dependence and a *ca.* 50-fold increase in K value was observed upon cooling the temperature from 55 °C to 10 °C. This larger change in K observed for Me_{18}-α-CD and I_3^- enlarged the concentration difference of free I_3^- between the cold- and hot-branches of the cell.

The enhancement in S_e can be attributed to the changes in association enthalpy, where an increase of −1 kcal mol^{-1} in ΔH increases the S_e by 0.06 mV K^{-1}. From Table S3,† the initial binding enthalpy ΔH_1 at 25 °C was −10.1 kcal mol^{-1} and the increment in S_e was estimated to be 0.6 mV K^{-1}. On the other hand, Me_{18}-α-CD enhanced the S_e of the thermocell to 1.08 mV K^{-1}. This discrepancy indicates that the association of I_5^- with Me_{18}-α-CD further increased the concentration difference of I_3^- between both branches of the cell, which further enhanced the Seebeck coefficient.

UV-vis spectroscopy

To investigate the species present in the mixed solution of I_2, KI and methyl-α-CD, UV-vis spectroscopy was executed (Fig. 5). The

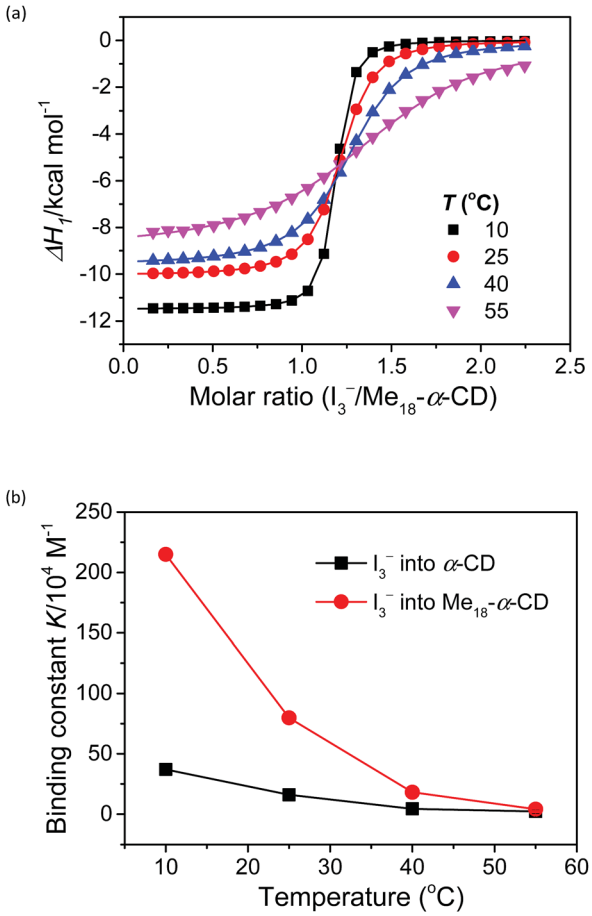

Fig. 4 (a) Initial binding enthalpy (ΔH_1 in Fig. 3b) of the ITC curves for Me_{18}-α-CD with I_3^- at various temperatures. (b) Temperature difference in the binding constant, *K*, observed for α-CD (black squares) and Me_{18}-α-CD (red circles) with I_3^-.

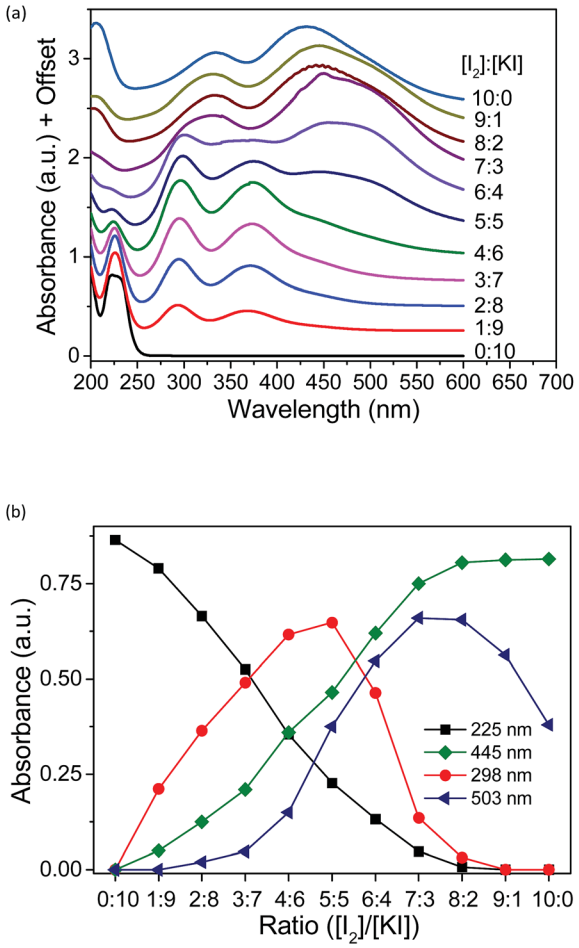

Fig. 5 (a) UV-vis spectra of aqueous solutions with varying concentrations. (b) Absorbance of all the peaks in the UV spectra plotted against the ratio of [I_2]/[KI]. [Me_{18}-α-CD] = 2.1 mM.

peaks were primarily assigned using reference solutions (Fig. S5†). As shown in Fig. S5,† an aqueous solution of pure KI has two peaks at 192 and 225 nm, which are attributed to the absorption peaks of I^-.[28,29] When I_2 was added to the KI solution, new peaks emerged at 290 and 352 nm, which reflect the formation of I_3^- ions through eqn (2).[28–32]

$$I_2 + I^- \rightleftharpoons I_3^- \quad (3)$$

A saturated I_2 solution without KI has four peaks at 205, 290, 352, and 460 nm, among which, the peaks at 205 and 460 nm are attributed to I_2.[28,29,31,32] The other two peaks at 290 and 352 nm are derived from the I_3^- ion generated by the hydrolysis of iodine, as described in the literature.[33–35] The α-CD–I_3^- complex formed upon the addition of α-CD to the aqueous mixture of KI and I_2 gave almost identical peaks at 290 and 353 nm.[25,26,35] Moreover, upon the addition of Me_{18}-α-CD, considerable red-shifts to 300 and 375 nm were observed (Fig. S5†), reflecting the complexation by Me_{18}-α-CD according to eqn (1). This red-shift in comparison with that of α-CD can be ascribed to the modified bond distance of I_3^- in the relatively deeper and more hydrophobic cavity of Me_{18}-α-CD, which may have affected the electronic structure of I_3^-.[36] The component observed for the mixture of I_2 and Me_{18}-α-CD at 430 nm is attributed to Me_{18}-α-CD–I_2, which is blue shifted due to the elevated LUMO level of I_2 by the interaction with the oxygen atoms of Me_{18}-α-CD.[37–40] Furthermore, a shoulder peak at 503 nm was observed in the spectrum (Fig. S5†), which has never been reported for the previous solution systems. In the solid state, the absorption at around 500 nm has been assigned to that of the I_5^- anion;[41–46] thus, we attribute the peak at 503 nm to Me_{18}-α-CD–I_5^-. The complex is formed through eqn (2).

$$Me_{18}\text{-α-CD–}I_3^- + I_3^- \rightleftharpoons Me_{18}\text{-α-CD–}I_5^- + I^- \quad (2)$$

The formation of Me_{18}-α-CD–I_5^- was further confirmed by Raman spectroscopy (Fig. S10†) *via* the increase in the I_2 stretching signal at *ca.* 170 cm^{-1}, which corresponds to I_5^- as an adduct of $I^- \cdot 2I_2$.[41,47–49]

As described above, Me_{18}-α-CD provides deeper hydrophobic cavity compared with that of α-CD (Fig. S1†), which must have stabilized the I_5^- species in the form of an Me_{18}-α-CD–I_5^-

complex. The assignment of the six peaks is summarized in Table S4.† The I_5^- ion has been found in solid polarizer films for liquid crystal displays, but to date, it has not been identified in aqueous solutions. Thus, the formation of Me_{18}-α-CD–I_5^- in aqueous solution provides a way to investigate the property of the discrete I_5^- ion.

The existing six peaks were further analyzed using Job's method.[50] The peaks in Fig. 5a correspond to I^- (225 nm), Me_{18}-α-CD–I_3^- (298 and 372 nm), Me_{18}-α-CD–I_2 (326 and 445 nm) and Me_{18}-α-CD–I_5^- (503 nm). These peaks were separated using Gaussian fitting and the peak intensities were plotted against the initial concentration ratio of I_2 and KI, as shown in Fig. 5b. The peak intensity of I^- at 225 nm monotonically decreased with an increase in the concentration ratio. Moreover, the absorbance of Me_{18}-α-CD–I_3^- at 298 nm increased almost proportionally at a low concentration of I_2. After reaching the maximum intensity at the ratio of 5 : 5, the peak at 298 nm decreased beyond that ratio. The peak at 445 nm (Me_{18}-α-CD–I_2) naturally showed a monotonic increase with an increase in I_2 concentration. The peak at 503 nm (Me_{18}-α-CD–I_5^-) showed the maximum at the $[I_2]/[KI]$ ratio of 7 : 3 to 8 : 2, and decreased beyond this ratio.

If the triiodide is the only polyiodide product in the aqueous mixture of KI and I_2, the plot of triiodide species (at 298 nm) should give a parabolic curve. The sharp decrease in Me_{18}-α-CD–I_3^- (298 nm) and increase in the Me_{18}-α-CD–I_5^- (503 nm) species between the ratio of 5 : 5 to 7 : 3 indicated that when the ratio of I_2 is higher than 5 : 5, Me_{18}-α-CD–I_3^- reacts with I_3^- to give the Me_{18}-α-CD–I_5^- complex through eqn (2).

Although molecular iodine is slightly soluble in water (1.18 mM, 20 °C),[51–53] no precipitation was observed in our experiments, even in the absence of added KI. This is attributed to the high water solubility of Me_{18}-α-CD–I_2 and formation of Me_{18}-α-CD–I_5^-. In addition, the weak acidity of the saturated iodine solution of pH 6.6 can be associated with the hydrolysis of iodine. The appearance of each solution is shown in Fig. S7.† The dark color of the 10 : 0 solution indicates the coexistence of Me_{18}-α-CD–I_2 and Me_{18}-α-CD–I_5^-.

Based on these spectral analyses, the concentration of the iodide species in the thermocell was then estimated by UV-vis spectroscopy. Fig. 6a shows the UV spectra with various concentrations of Me_{18}-α-CD at 25 °C. As discussed previously, the two peaks of I_3^- at 290 and 352 nm showed a red shift upon the addition of Me_{18}-α-CD, which corresponds to the formation of Me_{18}-α-CD–I_3^-. The other peaks at 445 and 503 nm are attributed to Me_{18}-α-CD–I_2 and Me_{18}-α-CD–I_5^-, respectively. Upon increasing the concentration of Me_{18}-α-CD, the intensity of the peaks at 445 and 503 nm increased and the color of the solution changed from yellow to deep red-black (Fig. S6†), which reflect the formation of Me_{18}-α-CD–I_5^-. Upon the addition of Me_{18}-α-CD at higher concentrations beyond 3 mM, the color of the solution returned to weak red (Fig. S6†). To understand these color changes, the intensity of the peaks was plotted in Fig. 6b with a variation in the concentration of the host. As the absorbance of I_3^- (290 nm) decreased, the absorption intensities of the Me_{18}-α-CD–I_3^- (372 nm) and Me_{18}-α-CD–I_2 (445 nm) species increased. The absorbance of

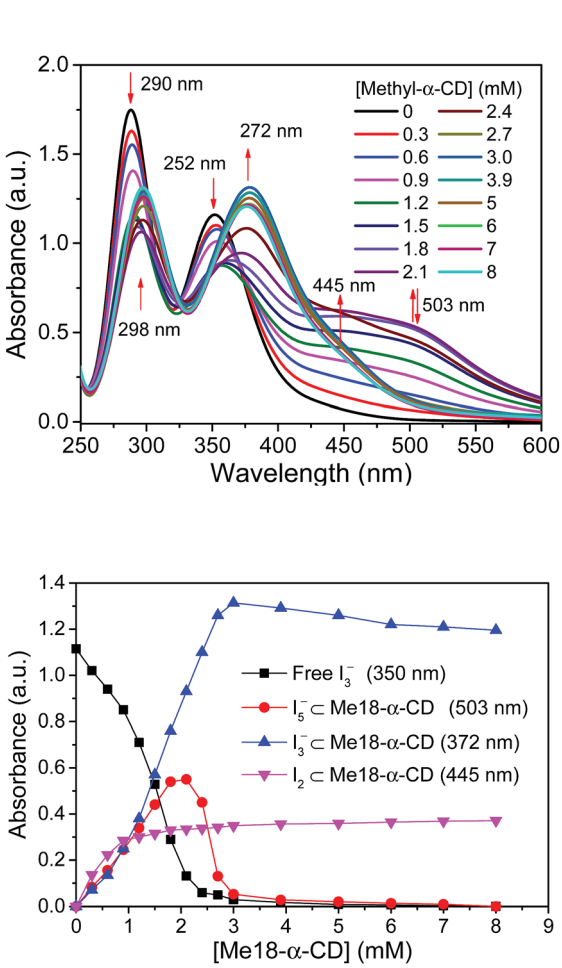

Fig. 6 (a) UV-vis spectra of solution 1 with various concentrations of Me_{18}-α-CD at 25 °C. (b) Plots of the peak absorbance of I_3^-, Me_{18}-α-CD–I_3^-, Me_{18}-α-CD–I_5^-, and Me_{18}-α-CD–I_2 in (a).

Me_{18}-α-CD–I_3^- and Me_{18}-α-CD–I_2 reached almost constant when the concentration of Me_{18}-α-CD was elevated to *ca.* 3 mM. The absorbance of Me_{18}-α-CD–I_5^- increased similarly to that of Me_{18}-α-CD–I_3^- below the Me_{18}-α-CD concentration of 2.1 mM, but it showed an abrupt decrease beyond this host concentration. This indicates that Me_{18}-α-CD–I_5^- underwent comproportionation to two Me_{18}-α-CD–I_3^- molecules according to eqn (4).[54–57]

$$Me_{18}\text{-α-CD–}I_5^- + Me_{18}\text{-α-CD} + I^- \rightleftharpoons 2Me_{18}\text{-α-CD–}I_3^- \quad (4)$$

The increase in the V_{OC} and S_e values of the thermocell may be associated with the concentration difference in free I_3^- ions between the lower- and higher-temperature half-cells, which undergo a reduction reaction in the thermocell.[18] Therefore, the temperature dependence of the concentration of free I_3^- was estimated by UV-vis spectroscopy under various host concentrations. All the spectra are revealed in Fig. S8,† and the peak intensity of free I_3^- species at 352 nm was estimated and plotted at various temperatures and Me_{18}-α-CD concentrations, as shown in Fig. 7a. At lower concentrations of Me_{18}-α-CD, a slight

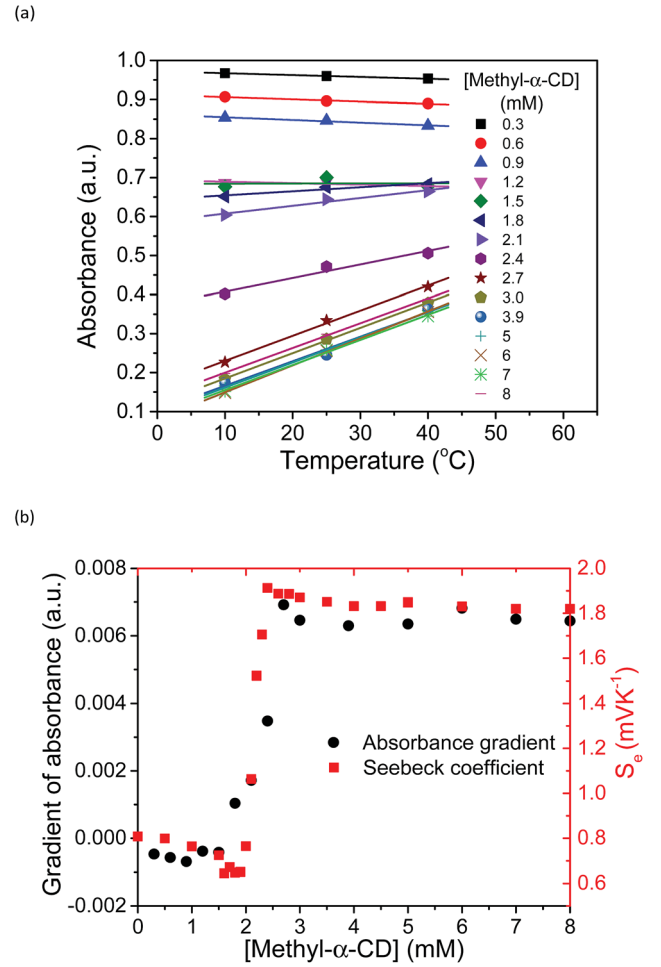

Fig. 7 (a) Temperature dependence of the absorbance of free I_3^- species at 352 nm at various concentrations of Me_{18}-α-CD at [KI] = 12.5 mM and $[I_2]$ = 2.5. The slope of the graph changes from negative to positive. (b) Temperature gradient of the UV peak at 352 nm and S_e at various concentrations of Me_{18}-α-CD, where they are in good agreement with each other.

decrease in the peak intensity was observed with an increase in temperature. The peak intensity of free I_3^- also decreased with an increase in the concentration of Me_{18}-α-CD. Upon an increase in temperature, a relatively large increase in the free I_3^- signal was observed for the aqueous Me_{18}-α-CD above the host concentration of 1.8 mM. This is ascribed to the decrease in the binding constant between Me_{18}-α-CD and I_3^- and the dissociation of the complex to liberate free I_3^- species by heating.

The slope of the lines in Fig. 7a at various Me_{18}-α-CD concentrations was plotted in Fig. 7b. The change in the slope drastically increased in the concentration range of 2.0 to 2.2 mM. The change in the I_3^- concentration affected the S_e, and the trend of the graph quite resembles the curve of S_e. Thus, the enhancement of S_e of the thermocell can be attributed to the host-guest interaction between Me_{18}-α-CD and I_3^-.

Temporal stability of the thermocell

The power output could be obtained by applying an external load voltage (V) to the thermocell (Fig. S11†) and measuring the I–V curves. The maximum power output at each condition was obtained from the plot of power and voltage (Fig. S11b†). The addition of the supporting electrolyte, KCl, to the supramolecular thermocell led to an increase in the current output, as reported previously.[18] However, in the previous study, precipitation emerged when pristine α-CD was used as the host matrix, and the power output drastically degraded in 6 h. This precipitation occurred due to the hydrogen bonding between the α-CD–I_3^- species, which is the fatal flaw for the long-term operation of α-CD-based thermocells. However, such precipitation was not observed when KCl was added to the aqueous mixture of Me_{18}-α-CD, I_2 and KI. Apparently, methylation of the hydroxy groups effectively prevented precipitation. Fig. 8 shows the time dependence of the power output obtained for the Me_{18}-α-CD-based supramolecular thermocell with and without KCl. As shown in this figure, a stable power output was observed, reflecting the stability of the Me_{18}-α-CD–I_3^- complex in aqueous media. The stable power output of the Me_{18}-α-CD–I_3^--based thermocell, normalized by the temperature difference, was 0.21 mW m^{-2} K^{-1}, which is *ca.* 2.3 times higher than that of the

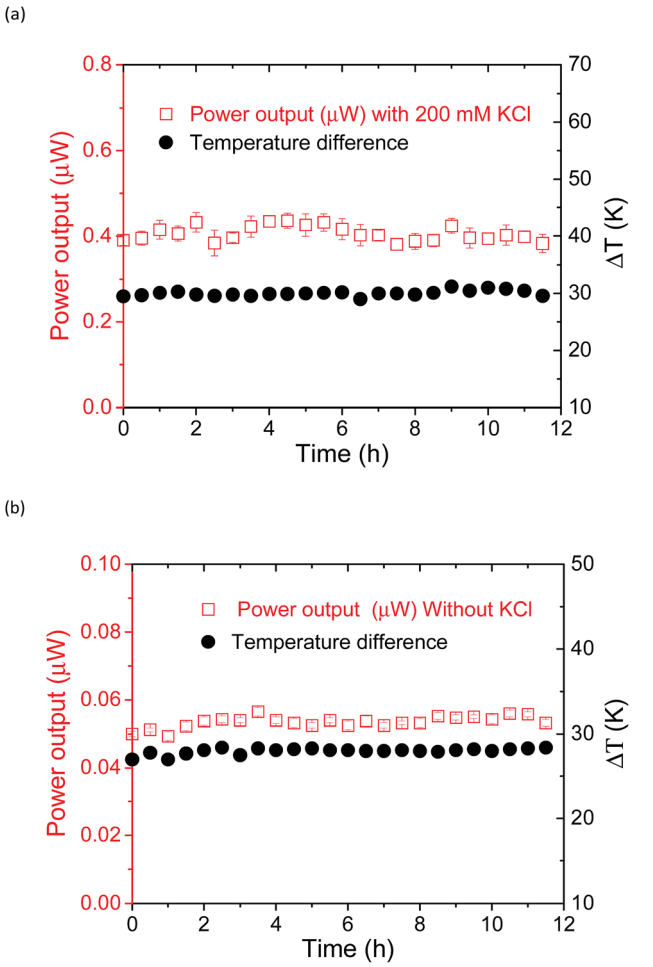

Fig. 8 Time dependence of the power output of the thermocell (KI = 12.5 mM, I_2 = 2.5 mM and Me_{18}-α-CD = 4 mM) with (a) and without (b) KCl. The temperature difference was controlled at *ca.* 29 K (a) and 30 K (b), which was monitored and added to these figures.

α-CD–I_3^--based thermocell after continuous operation for 6 h (0.09 mW m^{-2} K^{-1}).

Conclusions

Me_{18}-α-CD was added to an I^-/I_3^- thermocell and its Seebeck coefficient improved due to host–guest interactions. Compared with pristine α-CD, Me_{18}-α-CD showed stronger interaction with I_3^-, and the S_e of the thermocell was enhanced up to 1.9 mV K^{-1} without precipitation. The observed S_e value is the highest reported for pure-water thermocell systems to date.

UV-vis spectroscopy revealed that I_5^- was captured in the aqueous Me_{18}-α-CD, in addition to Me_{18}-α-CD–I_3^-. This result is the first observation of I_5^- formed in an aqueous system. The binding constants of Me_{18}-α-CD and I_3^- were estimated by ITC measurement. The estimated enhancement of S_e was *ca.* 0.6 mV K^{-1}. The additional enhancement of S_e was derived from the formation of I_5^-, which boosted the concentration difference between the hot and cold branches of the cell. The thermal change in the free I_3^- concentration was evaluated by UV-vis measurement, which resembled the S_e trend. The methylation of the hydroxyl groups in Me_{18}-α-CD effectively prevented the formation of the hydrogen-bonded polymer complexes observed for the α-CD–I_3^- complex. As a result, the absence of precipitation in the present Me_{18}-α-CD/I_3^- system offered high durability, which was a critical issue in the previous α-CD–I_3^- system. These results indicate that the precise design of the host–guest interaction is imperative to improve the performance of thermocells.

Conflicts of interest

There are no conflicts to declare.

Acknowledgements

This study was partly supported by JST PRESTO Grant Number JPMJPR141D, Japan and JSPS KAKENHI Grant Numbers JP25220805, JP17H03046, JP26708007 and JP16H06513 (Coordination Asymmetry). The authors gratefully acknowledge the support of ITC measurement from Dr Yu Hoshino (Department of Chemical Engineering, Graduate School of Engineering, Kyushu University).

Notes and references

1 K. Biswas, J. He, I. D. Blum, C.-I. Wu, T. P. Hogan, D. N. Seidman, V. P. Dravid and M. G. Kanatzidis, *Nature*, 2012, **489**, 414–418.
2 L. M. Goncalves, P. Alpuim and J. H. Correia, *J. Electron. Mater.*, 2010, **39**, 1516–1521.
3 A. R. M. Siddique, S. Mahmud and B. Van Heyst, *Renewable Sustainable Energy Rev.*, 2017, **73**, 730–744.
4 T. C. Harman, M. P. Walsh, B. E. Laforge and G. W. Turner, *J. Electron. Mater.*, 2005, **34**, L19–L22.
5 G. Jeffrey Snyder and E. S. Toberer, *Nat. Mater.*, 2008, **7**, 105–114.
6 T. I. Quickenden and Y. Mua, *J. Electrochem. Soc.*, 1995, **142**, 3985–3994.
7 A. Gunawan, C. H. Lin, D. A. Buttry, V. Mujica, R. A. Taylor, R. S. Prasher and P. E. Phelan, *Nanoscale Microscale Thermophys. Eng.*, 2013, **17**, 304–323.
8 L. Zhang, T. Kim, N. Li, T. J. Kang, J. Chen, J. M. Pringle, M. Zhang, A. H. Kazim, S. Fang, C. Haines, D. Al-Masri, B. A. Cola, J. M. Razal, J. Di, S. Beirne, D. R. MacFarlane, A. Gonzalez-Martin, S. Mathew, Y. H. Kim, G. Wallace and R. H. Baughman, *Adv. Mater.*, 2017, **29**, 1605652.
9 Y. Mua and T. I. Quickenden, *J. Electrochem. Soc.*, 1996, **143**, 2558–2564.
10 T. I. Quickenden and C. F. Vernon, *Sol. Energy*, 1986, **36**, 63–72.
11 M. F. Dupont, D. R. MacFarlane and J. M. Pringle, *Chem. Commun.*, 2017, **53**, 6288–6302.
12 R. Hu, B. A. Cola, N. Haram, J. N. Barisci, S. Lee, S. Stoughton, G. Wallace, C. Too, M. Thomas, A. Gestos, M. E. Dela Cruz, J. P. Ferraris, A. A. Zakhidov and R. H. Baughman, *Nano Lett.*, 2010, **10**, 838–846.
13 H. Im, T. Kim, H. Song, J. Choi, J. S. Park, R. Ovalle-Robles, H. D. Yang, K. D. Kihm, R. H. Baughman, H. H. Lee, T. J. Kang and Y. H. Kim, *Nat. Commun.*, 2016, **7**, 10600.
14 M. S. Romano, N. Li, D. Antiohos, J. M. Razal, A. Nattestad, S. Beirne, S. Fang, Y. Chen, R. Jalili, G. G. Wallace, R. Baughman and J. Chen, *Adv. Mater.*, 2013, **25**, 6602–6606.
15 T. J. Abraham, D. R. MacFarlane and J. M. Pringle, *Energy Environ. Sci.*, 2013, **6**, 2639–2645.
16 T. J. Abraham, D. R. MacFarlane and J. M. Pringle, *Chem. Commun.*, 2011, **47**, 6260–6262.
17 T. Kim, J. S. Lee, G. Lee, H. Yoon, J. Yoon, T. J. Kang and Y. H. Kim, *Nano Energy*, 2017, **31**, 160–167.
18 H. Zhou, T. Yamada and N. Kimizuka, *J. Am. Chem. Soc.*, 2016, **138**, 10502–10507.
19 H. Zhou, T. Yamada and N. Kimizuka, *Sustainable Energy Fuels*, 2018, **2**, 472–478.
20 E. M. Nour, L. H. Chen and J. Laane, *J. Phys. Chem.*, 1986, **90**, 2841–2846.
21 E. E. Havinga and E. H. Wiebenga, *Acta Crystallogr.*, 1958, **11**, 733–737.
22 R. J. Hach and R. E. Rundle, *J. Am. Chem. Soc.*, 1951, **73**, 4321–4324.
23 F. H. Herbstein and M. Kapon, *Nature Phys. Sci.*, 1972, **239**, 153–154.
24 S. Kitamura, K. Nakatani, T. Takaha and S. Okada, *Macromol. Rapid Commun.*, 1999, **20**, 612–615.
25 J. L. Pursell and C. J. Pursell, *J. Phys. Chem. A*, 2016, **120**, 2144–2149.
26 J. W. Minns and A. Khan, *J. Phys. Chem. A*, 2002, **106**, 6421–6425.
27 W. Kim, Y. Yamasaki and K. Kataoka, *J. Phys. Chem. B*, 2006, **110**, 10919–10925.
28 S. V. Kireev and S. L. Shnyrev, *Laser Phys.*, 2015, **25**, 75602.
29 Y. J. Wei, L. C. Ge and L. P. Mo, *Spectrosc. Spectr. Anal.*, 2005, **25**, 86–88.
30 Y. Bichsel and U. Von Gunten, *Anal. Chem.*, 1999, **71**, 34–38.

31 D. A. Palmer, R. W. Ramette and R. E. Mesmer, *J. Solution Chem.*, 1984, **13**, 673–683.
32 R. C. Troy, M. D. Kelley, J. C. Nagy and D. W. Margerum, *Inorg. Chem.*, 1991, **30**, 4838–4845.
33 I. Lengyel, I. R. Epstein and K. Kusth, *Inorg. Chem.*, 1993, **32**, 5880–5882.
34 J. W. Minns and A. Khan, *J. Phys. Chem. A*, 2002, **106**, 6421–6425.
35 V. Calabrese and A. Khan, *J. Phys. Chem. A*, 2000, **104**, 1287–1292.
36 D. L. Mould, *Biochem. J.*, 1954, **58**, 593–600.
37 R. S. Mulliken, *J. Am. Chem. Soc.*, 1950, **72**, 600–608.
38 R. P. Lang, *J. Am. Chem. Soc.*, 1962, **84**, 1185–1191.
39 K. H. Kim, H. Ki, J. H. Lee, S. Park, Q. Kong, J. Kim, J. Kim, M. Wulff and H. Ihee, *Phys. Chem. Chem. Phys.*, 2015, **17**, 8633–8637.
40 C. Reichardt, *Chem. Rev.*, 1994, **94**, 2319–2358.
41 P. H. Svensson and L. Kloo, *Chem. Rev.*, 2003, **103**, 1649–1684.
42 H. Kim, *Biopolymers*, 1982, **21**, 2083–2096.
43 W. Saenger, *Naturwissenschaften*, 1984, **71**, 31–36.
44 E. H. Wiebenga, E. E. Havinga and K. H. Boswijk, *Advances inoganic Chem. Radiochem.*, 1961, vol. 3, pp. 133–169.
45 M. Mizuno, J. Tanaka and I. Harada, *J. Phys. Chem.*, 1981, **85**, 1789–1794.
46 M. Noltermeyer and W. Saenger, *Nature*, 1976, **259**, 629–632.
47 P. Deplano, J. R. Ferraro, M. L. Mercuri and E. F. Trogu, *Coord. Chem. Rev.*, 1999, **188**, 71–95.
48 P. H. Svensson and L. Kloo, *Chem. Rev.*, 2003, **103**, 1649–1684.
49 L. A. Bengtsson, H. Stegemann, B. Holmberg and H. Füllbier, *Mol. Phys.*, 1991, **73**, 283–296.
50 P. Job, *Ann. Chim. Appl.*, 1928, **9**, 113.
51 L. I. Katzin and E. Gebert, *J. Am. Chem. Soc.*, 1955, **77**, 5814–5819.
52 F. C. Kracek, *J. Phys. Chem.*, 1931, **35**, 417–422.
53 D. Diaz, I. Vargas-Baca and J. Gracia-Mora, *J. Chem. Educ.*, 1994, **71**, 708–714.
54 L. Martin, S. Yang, A. C. Brooks, P. N. Horton, L. Male, O. Moulfi, L. Harmand, P. Day, W. Clegg and W. Harrington, *CrystEngComm*, 2015, **17**, 7354–7362.
55 C. A. Filgueiras, J. A. Horn, J. M. Skakle and J. L. Wardell, *Acta Crystallogr., Sect. E: Struct. Rep. Online*, 2001, **57**, o338–o340.
56 A. J. Blake, F. A. Devillanova, R. O. Gould, W. Li, S. Parsons and M. Schr, *Chem. Soc. Rev.*, 1998, **27**, 195–205.
57 L. Kloo, H. Svensson and M. J. Taylor, *J. Chem. Soc., Dalton Trans.*, 2000, **7**, 1061–1065.